J Ginseng Res 42 (2018) 512–523

Contents lists available at ScienceDirect

Journal of Ginseng Research

journal homepage: http://www.ginsengres.org

Research article

# Microemulsion-based hydrogels for enhancing epidermal/dermal deposition of topically administered 20(*S*)-protopanaxadiol: *in vitro* and *in vivo* evaluation studies

Ki-Taek Kim [1], Min-Hwan Kim [1], Ju-Hwan Park [1], Jae-Young Lee [2], Hyun-Jong Cho [3], In-Soo Yoon [4,**], Dae-Duk Kim [1,*]

[1] College of Pharmacy and Research Institute of Pharmaceutical Sciences, Seoul National University, Seoul, Republic of Korea
[2] College of Pharmacy, Chungnam National University, Daejeon, Republic of Korea
[3] College of Pharmacy, Kangwon National University, Gangwon, Republic of Korea
[4] College of Pharmacy, Pusan National University, Busan, Republic of Korea

ARTICLE INFO

*Article history:*
Received 18 April 2017
Received in Revised form
29 June 2017
Accepted 14 July 2017
Available online 18 August 2017

*Keywords:*
hairless mouse
microemulsion-based hydrogel (MEH)
20(*S*)-protopanaxadiol (20*S*-PPD)
Strat-M membrane
topical delivery

ABSTRACT

*Background:* 20(*S*)-Protopanaxadiol (20*S*-PPD) is a fully deglycosylated ginsenoside metabolite and has potent dermal antiaging activity. However, because of its low aqueous solubility and large molecular size, a suitable formulation strategy is required to improve its solubility and skin permeability, thereby enhancing its skin deposition. Thus, we optimized microemulsion (ME)-based hydrogel (MEH) formulations for the topical delivery of 20*S*-PPD.

*Methods:* MEs and MEHs were formulated and evaluated for their particle size distribution, morphology, drug loading capacity, and stability. Then, the deposition profiles of the selected 20*S*-PPD-loaded MEH formulation were studied using a hairless mouse skin model and Strat-M membrane as an artificial skin model.

*Results:* A Carbopol-based MEH system of 20*S*-PPD was successfully prepared with a mean droplet size of 110 nm and narrow size distribution. The formulation was stable for 56 d, and its viscosity was high enough for its topical application. It significantly enhanced the *in vitro* and *in vivo* skin deposition of 20*S*-PPD with no influence on its systemic absorption in hairless mice. Notably, it was found that the Strat-M membrane provided skin deposition data well correlated to those obtained from the *in vitro* and *in vivo* mouse skin studies on 20*S*-PPD (correlation coefficient $r^2 = 0.929–0.947$).

*Conclusion:* The MEH formulation developed in this study could serve as an effective topical delivery system for poorly soluble ginsenosides and their deglycosylated metabolites, including 20*S*-PPD.



## 1. Introduction

Among a number of active constituents of ginseng, ginsenosides are known to be responsible for the diverse pharmacological effects of ginseng [1]. However, only a few studies have focused on the therapeutic and cosmeceutical potential of ginsenosides for skin healthcare. Ginsenosides Rb1 and F1 have been reported to show antimelanogenic activity in B16 cells and human skin, respectively [2,3]. More recently, a compound K (known as a partially deglycosylated ginsenoside metabolite)-rich fraction prepared from ginseng was demonstrated to have antiphotoaging activity via the modulation of several signaling pathways in UV-B-irradiated NIH3T3 fibroblasts and alpha-melanocyte-stimulating hormone-treated B16F10 cells [4]. However, those studies used classic formulations, such as solutions and creams, for the topical application of ginsenosides. The limited solubility and membrane permeability of relevant ginsenosides [5–7] warrant further studies on the

* Corresponding author. College of Pharmacy and Research Institute of Pharmaceutical Sciences, Seoul National University, 1 Gwanak-ro, Gwanak-gu, Seoul 08826, Republic of Korea.
** Corresponding author. College of Pharmacy, Pusan National University, 2 Busandaehak-ro 63 beon-gil, Geumjeong-gu, Busan 46241, Republic of Korea.
*E-mail addresses:* insoo.yoon@pusan.ac.kr (I.-S. Yoon), ddkim@snu.ac.kr (D.-D. Kim).

http://dx.doi.org/10.1016/j.jgr.2017.07.005
p1226-8453 e2093-4947/$ – see front matter 

development of more efficient cosmeceutical ginsenoside preparations using suitable topical delivery systems.

20(*S*)-Protopanaxadiol (20*S*-PPD; Fig. 1) is a fully deglycosylated metabolite of ginsenosides Rb1, Rb2, Rb3, Rg3, Rh2, and compound K [8]. It has various pharmacological activities including antiestrogen, cardioprotective, antitumor, anti-inflammatory, and antidepressant effects [9]. Currently, a 20*S*-PPD capsule is being developed as a novel antidepressant and is undergoing phase-IIa clinical trials in China [9]. Notably, a recent study demonstrated that 20*S*-PPD showed markedly higher antiwrinkle and skin-whitening effects in immortalized human keratinocytes and 3D-cultured human skin equivalent models than compound K and Rb1 did, via the suppression of matrix metalloproteinases, which mediates the degradation of collagen and elastin in the skin [10]. However, there have been no published studies on the topical delivery of 20*S*-PPD so far. Moreover, 20*S*-PPD has a low aqueous solubility (<50 ng/mL) and relatively large molecular size (460.7 Da), which would be the main obstacles to its permeation through the stratum corneum (SC) and deposition in the epidermis and dermis [11]. Therefore, a suitable formulation strategy is required to improve the solubility and skin permeability of 20*S*-PPD to enhance its epidermal/dermal deposition.

Among the various pharmaceutical dosage forms, microemulsion (ME) has emerged as a promising nano-sized carrier system for the topical delivery of drugs with low solubility and/or low permeability [12–14]. MEs are composed of an oil phase, water phase, and surfactant mixture ($S_{mix}$), which is an isotropic, transparent, and thermodynamically stable colloidal system with droplet sizes ranging from 10 nm to 200 nm [15,16]. Water-insoluble drugs can be solubilized in the oil phase and/or adsorbed into the oil–water interface of an ME, which allows a higher drug loading capacity of the ME formulation and enhances the driving force of drug permeation through the skin [17,18]. Moreover, several ingredients of the ME formulation can serve as permeation enhancers to overcome skin barrier functions [19]. However, despite the advantages of MEs, its topical application in a clinical setting has often been hindered because of its low viscosity [15]. Thus, ME-based hydrogels (MEHs) have attracted interest as an alternative topical delivery system [15,17,20,21]. In general, MEHs with a suitable viscosity and good biocompatibility can prolong the retention time of drug on the skin and reduce the risk of skin irritation after their topical application [22,23].

Therefore, the objective of the present study was to investigate the feasibility of applying pharmaceutical drug delivery technology to the topical delivery of 20*S*-PPD using MEs and MEHs. The 20*S*-PPD-loaded ME and MEH formulations were prepared via the construction of a pseudo ternary phase diagram and characterized *in vitro* in terms of loading capacity, particle-size distribution, morphology, surface charge, viscosity, and long-term stability. Then, the *in vitro* and *in vivo* skin deposition properties were studied using hairless mice and Strat-M membranes, an artificial skin membrane. Additionally, the correlation between the skin deposition profiles of 20*S*-PPD in hairless mouse skin and Strat-M membrane was investigated.

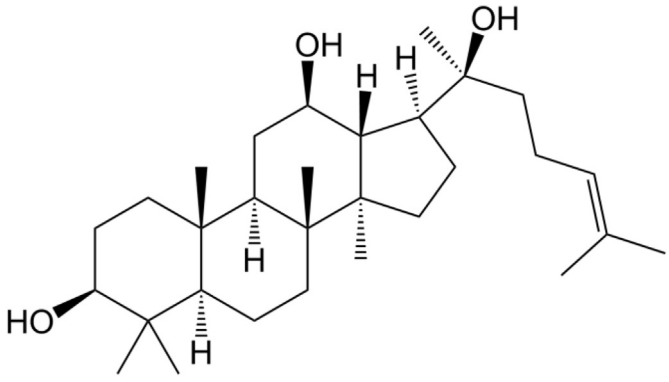


**Fig. 1.** Chemical structure of 20(*S*)-protopanaxadiol (20*S*-PPD). Orally administered ginsenosides Rb1, Rb2, Rb3, Rg3, Rh2, and compound K can be deglycosylated by intestinal bacteria or digestive enzyme and converted to 20*S*-PPD, a fully deglycosylated ginsenoside metabolite.

## 2. Materials and methods

### 2.1. Materials

20*S*-PPD (purity ≥ 98.0%) was purchased from Xian Plant Bio-Engineering Co., Ltd. (Shaanxi, China). Capmul MCM EP was gifted by ABITEC Co. (Peterborough, UK). Labrafac CC, Lauroglycol CC, Labrasol (PEG-8 caprylic/capric glycerides), and Transcutol HP were gifted by Gattefossé Co. (Saint Priest, Cedex, France). Tween 20, isopropyl myristate, limonene, polyethylene glycol 400 (PEG400), sodium lauryl sulfate, soybean phosphatidyl-choline (soy PC), xanthan gum, triethanolamine, and ketoprofen were purchased from Sigma-Aldrich Chemical Co. (St. Louis, MO, USA). Poloxamer 407 was obtained from BASF Co. (Ludwigshafen, Germany). Carbopol 941 was obtained from the Lubrizol Co. (Wickliffe, OH, USA). Phosphate buffered saline was purchased from Lonza, Ltd. (Basel, Switzerland). HPLC-grade methanol and acetonitrile were purchased from Thermo Fisher Scientific Co. (Pittsburgh, PA, USA).

### 2.2. Animals

For *in vitro* and *in vivo* evaluation, male hairless mice (5 wk of age, 20–25 g) were used and obtained from Orient Bio Inc. (Sungnam, Korea). They were housed on sawdust, and five mice were in each cage. They had free access to water and food prior to the study. The room was maintained under a 12-h automatic cycle of light/darkness, and the room temperature was maintained at 25 ± 2°C. They were acclimatized to these conditions for at least 1 wk before the experiments began. Experimental protocols for the animals (Approval number: SNU-111007-4-2) used in this study were reviewed by the Animal Care and Use Committee of the College of Pharmacy, Seoul National University, and were in accordance with the National Institutes of Health's Guide for the Care and Use of Laboratory Animals (National Institutes of Health Publication Number 85-23, revised 1985).

### 2.3. Preparation of 20S-PPD-loaded ME and MEH formulations

#### 2.3.1. Solubility study

The solubility of 20*S*-PPD was determined in various vehicles by adding an excessive amount of 20*S*-PPD into a tube containing 1 mL of each vehicle. The mixtures were allowed to approach an equilibrium state in a vortex shaker (Vortex-Genie 2; Scientific Industries, Inc., Bohemia, NY, USA) at 50 rpm at 25°C for 72 h. The samples were centrifuged at 16,000*g* for 5 min, and the supernatant was passed through a 0.20-μm syringe filter to remove excess 20*S*-PPD. Finally, the concentration of 20*S*-PPD in the filtered solution was quantified by LC–MS/MS after appropriate dilution with methanol.

#### 2.3.2. Construction of pseudo-ternary phase diagrams

Based on the results of the solubility test (Table 1), Capmul MCM EP was selected as the oil phase, whereas Labrasol and Tween 20 were selected as the surfactant mixture ($S_{mix}$) phase. For the construction of pseudo-ternary phase diagram, the combination of surfactants (Labrasol and Tween 20) were mixed at various ratios

**Table 1**
Solubility (ng/mL for DW and mg/mL for the others) of 20*S*-PPD in various vehicles ($n = 3$)

| Phase | Vehicle | Solubility |
|---|---|---|
| Water | DW | 36.8 ± 4.83 |
| Oil | Capmul MCM EP | 10.6 ± 1.44 |
| | Lauroglycol CC | 6.87 ± 0.380 |
| | Labrafac CC | 3.80 ± 0.820 |
| Surfactant | Labrasol | 8.63 ± 1.78 |
| | Tween 20 | 5.37 ± 0.887 |
| | Isopropyl myristate | 2.53 ± 0.734 |
| | Limonene | 1.54 ± 0.258 |
| | PEG 400 | 0.0152 ± 0.00487 |

DW, distilled water; 20*S*-PPD, 20(*S*)-protopanaxadiol.

(1:1, 2:1, and 3:1, w/w) to make the $S_{mix}$. Then, the oil phase and $S_{mix}$ were mixed at 9:1, 8:2, 7:3, 6:4, 5:5, 4:6, 3:7, 2:8, and 1:9 (w/w). Distilled water (DW) was added dropwise to each oil and $S_{mix}$ combination at room temperature while stirring to allow equilibration. After equilibrium, the mixtures were visually checked for transparency. The points from clear to turbid state are presented in Fig. 2.

### 2.3.3. Preparation of 20*S*-PPD-loaded ME and MEH formulations

From the clear region of pseudo-ternary phase diagrams, three ME formulations (F1–F3) were selected for further evaluations (Table 2). For the preparation of MEs with 0.1% (w/w) 20*S*-PPD, the exact amount of 20*S*-PPD was first added into the Capmul MCM EP and vortex-mixed to dissolve 20*S*-PPD. Labrasol and Tween 20 mixtures were subsequently added to the 20*S*-PPD oil solution under gentle stirring at room temperature. Then, DW was added dropwise into the above mixture under the same conditions. To investigate the synergic effect of cosurfactants Transcutol HP and soy PC, they were added into the $S_{mix}$, after the 20*S*-PPD was added in the Capmul MCM EP and DW was added as described above (F4 and F5, Table 2). To prepare MEHs of 20*S*-PPD, three different

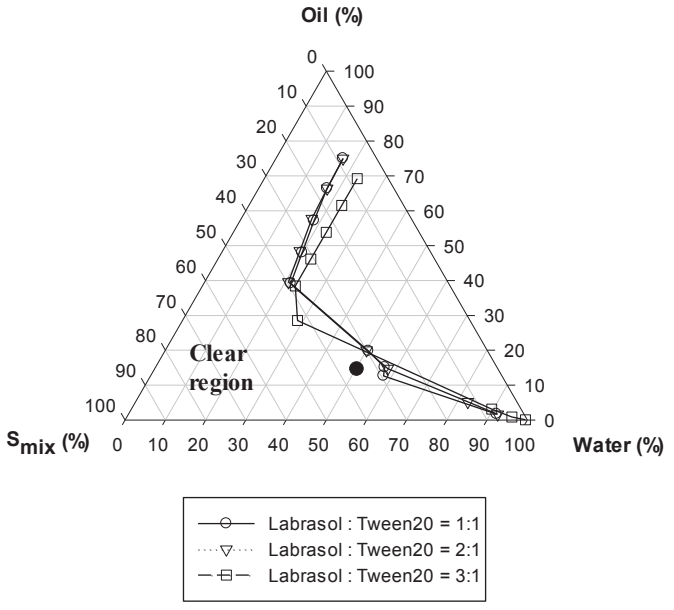


**Fig. 2.** Pseudo-ternary phase diagrams of water, Capmul MCM EP (oil), and surfactant mixture ($S_{mix}$). The $S_{mix}$ is a combination of Labrasol and Tween 20 at 1:1, 2:1, and 3:1 (w/w). Transparent microemulsions (MEs) were formed in the clear region, whereas the other region represents turbid emulsions. The closed circle represents the compositions of ME formulations prepared with the three different $S_{mix}$ ratios (1:1, 1:2, and 1:3 for F1, F2, and F3, respectively).

**Table 2**
Weight compositions of ME formulations containing 0.1% (w/w) 20*S*-PPD

| | Water | Oil | Surfactant | | Cosurfactant | |
|---|---|---|---|---|---|---|
| | DW | Capmul MCM EP | Labrasol | Tween 20 | Transcutol | Soy PC |
| F1 | 47.5 | 17.5 | 17.5 | 17.5 | | |
| F2 | 47.5 | 17.5 | 23.3 | 11.7 | | |
| F3 | 47.5 | 17.5 | 26.2 | 8.8 | | |
| F4 | 42.5 | 17.5 | 17.5 | 17.5 | 5.0 | |
| F5 | 41.5 | 17.5 | 17.5 | 17.5 | 5.0 | 1.0 |

ME, microemulsion; 20*S*-PPD, 20(*S*)-protopanaxadiol; soy PC, soybean phosphatidyl-choline.

hydrophilic polymers (xanthan gum, Poloxamer 407, and Carbopol 941) were added at 1.0%, 15.0%, and 1.0% (w/w), respectively, in the F5 formulation (F5-H), where the Carbopol 941-based MEH was neutralized with 2.0% (w/w) triethanolamine.

### 2.4. Characterization of 20*S*-PPD-loaded ME and MEH formulations

The mean particle size, polydispersity index, intensity distribution of particle size, and zeta potential of 20*S*-PPD-loaded MEs were measured in triplicate by an electrophoretic light-scattering (ELS) spectrophotometer (ELS 8000; Otsuka Electronics Co. Ltd., Tokyo, Japan). The 20*S*-PPD-loaded MEs were transferred to a quartz cuvette, and all measurements were performed at 25°C.

The particle morphologies of the 20*S*-PPD-loaded MEs and MEHs were observed by an energy-filtering transmission electron microscopy (TEM; LIBRA 120; Carl Zeiss, Jena, Germany) at 80 kV. The samples were placed on a carbon-coated copper grid and negatively stained with 2% phosphotungstic acid followed by drying at room temperature prior to the operation.

The pH values of the 20*S*-PPD-loaded MEs and MEHs were evaluated using a pH meter (OrionTM 3-Star Benchtop; Thermo Fisher Scientific Co.) at 25°C in triplicate after calibration with standard pH buffer solutions ranging from pH 4.0 to 10.0.

The viscosity of the 20*S*-PPD-loaded MEs and MEHs was evaluated using a rotational viscosity measurement device coupled with a concentric cylinder (LV1) at 25°C (Brookfield viscometer LVDVE; Brookfield Engineering Laboratories, Inc., Middleboro, MA, USA).

To confirm the maximum 20*S*-PPD-loading capacity of the ME and MEH formulations, excess 20*S*-PPD was added into the combined oil and $S_{mix}$, after which the 20*S*-PPD-loaded MEs and MEHs were prepared. Next, excess 20*S*-PPD not included in the droplets of the ME was removed by centrifugation for 5.0 min at 16,000*g*. The supernatant was then injected into an LC–MS/MS system for analysis after adequate dilution with methanol.

### 2.5. In vitro deposition studies using hairless mouse skin and artificial membrane

*In vitro* deposition of 20*S*-PPD into hairless mouse skin was evaluated using Keshary–Chien diffusion cells at 32°C, which have a surface area of 1.77 $cm^2$ [24]. After sacrificing the mice by cervical dislocation, the dorsal skin was cut to an appropriate size and the subcutaneous fat was removed. Then, they were fixed between the donor and receptor cells, laying the SC toward the donor cells. The receptor cells were filled with phosphate buffered saline containing 1.0% w/v sodium lauryl sulfate (13.0 mL). Subsequently, various 20*S*-PPD-loaded MEs (F1 to F5) were applied to the donor cell side and sealed with parafilm to avoid evaporation of the samples. The skin was removed from the diffusion cells 6 h after applying the samples and washed out with methanol.

To determine the amount of 20*S*-PPD in the SC, the tape stripping method was used [25]. Cellophane adhesive tape (CuDerm Co., Dallas, TX, USA) was applied three times to the SC, and each tape was separately collected into a 2.0-mL tube. After removing the SC, the skin samples (i.e., epidermis and dermis) were chopped and collected in a mortar. The chopped samples were ground to a powder using a pestle after adding liquid nitrogen. The skin powders were collected with cellophane adhesive tape and transferred into a 2.0-mL tube. For the extraction of 20*S*-PPD from the tape, methanol (1.5 mL) was added and the tube was shaken for 3 h, followed by centrifugation for 5.0 min at 16,000*g*.

*In vitro* deposition of 20*S*-PPD into a Strat-M membrane was evaluated using the same diffusion cell. Strat-M membranes (2.5 cm diameter) were fixed between the donor and receptor cells, laying the shiny side toward the donor cells. The receptor cells were filled with the same media as described above. Then, 20*S*-PPD in various vehicles (0.1%, w/w), i.e., MEs (F1 to F5), MEH (F5-H), suspension (DW and propylene glycol mixture; 9:1 w/w), and oil (Capmul MCM EP) solution, was applied to the donor cell side and sealed with parafilm to avoid evaporation of the samples. The Strat-M membranes were removed from the diffusion cells 3 h after applying the samples and washed out with methanol. Then, they were placed into a 2.0-mL tube and a mixture of acetone and methanol (70:30 v/v%, 1.5 mL) was added. For the extraction of 20*S*-PPD from the Strat-M membrane, the tube was shaken for 3 h, followed by centrifugation for 5.0 min at 16,000*g*. Then, a 1.0-mL aliquot of the supernatant was evaporated using a gentle nitrogen gas stream at 30°C and reconstituted with 0.5 mL methanol. Finally, the amount of 20*S*-PPD in the SC at 6 h and epidermis/dermis of hairless mouse skin at 3 h and Strat-M membrane was analyzed using LC–MS/MS system. The deposited amount value of 20*S*-PPD was normalized by the skin surface area, with a dimension of ng/cm$^2$. This parameter was converted to the epidermal/dermal concentration value, with a dimension of nM, using the thickness of the epidermis/dermis layer of male hairless mouse skin (510 μm = 0.051 cm) and the molecular weight of 20*S*-PPD (460.7 g/mol).

### 2.6. In vivo skin deposition and plasma pharmacokinetic studies

*In vivo* skin deposition and permeation of 20*S*-PPD were evaluated using male hairless mice. The mice were slightly anesthetized with ether prior to the experiment and fixed with the dorsal part upward. To apply the suspension (DW and propylene glycol mixture; 9:1 w/w) and oil (Capmul MCM EP) solution, a specially designed cylinder-type chamber with a diffusion area of 0.79 cm$^2$ was put on the dorsal skin of the mice and fixed with surgical glue (Vet bond; 3M Co., St. Paul, MN, USA). After recovery from anesthesia, the suspension or oil solution containing 0.1% (w/w) of 20*S*-PPD was applied into the chamber to test the topical administration of 20*S*-PPD. In addition, a 20*S*-PPD-loaded MEH (F5-H) was applied on the same area by hand rubbing. All formulations were applied to the skin at a dose of 25 mg/kg.

Prior to sacrificing the mice at 3 h, 6 h, 12 h, 18 h, and 24 h, a 300-μL aliquot of blood was collected for evaluation of permeated 20*S*-PPD through the skin. Plasma samples were obtained by centrifugation for 5.0 min at 16,000 × *g* and stored at −20°C until LC–MS/MS analysis. The hairless mice were then sacrificed by cervical dislocation. Afterward, the skin samples were pretreated as described in the *in vitro* skin deposition study to determine the deposited 20*S*-PPD into the skin using LC–MS/MS system.

### 2.7. Stability test

The stability of 20*S*-PPD was evaluated by comparing the 20*S*-PPD content and change of particle size distribution in various formulations at room temperature and 40°C for 7 d, 14 d, 28 d, and 56 d. Briefly, an oil solution, 20*S*-PPD-loaded MEs (F1 and F5) and MEH (F5-H) containing 0.1% (w/w) of 20*S*-PPD were prepared and stored at the above conditions. At 0 d (initial state), 7 d, 14 d, 28 d, and 56 d, the mean particle size distribution of the samples was measured using an ELS spectrophotometer. To determine the 20*S*-PPD content, the samples were centrifuged for 5.0 min at 16,000*g*, and the supernatant was injected into an LC–MS/MS system after adequate dilution with methanol.

### 2.8. LC–MS/MS analysis of 20S-PPD

The amount of 20*S*-PPD was determined by LC–MS/MS analysis as previously described [9]. The samples were injected into an Agilent LC–MS/MS system (Agilent Technologies, Santa Clara, CA, USA) equipped with an Agilent Technologies 1260 Infinity HPLC system and Agilent Technologies 6430 Triple Quad LC–MS system. The samples were injected through a Hypersil BDS C18 column (50 mm × 4.6 mm, 5μm; Thermo Fisher Scientific Co.). The mobile phase was 93% acetonitrile and 7% water containing 0.2% formic acid (v/v). The flow rate was 0.37 mL/min. 20*S*-PPD was determined in the multiple reaction-monitoring mode with positive electrospray ionization. The gas temperature, gas flow, nebulizer pressure, and capillary voltage were 120°C, 9 L/min, 25 psi, and 6,000 V, respectively. The *m/z* value of the precursor to product ion, fragment voltage, collision energy, and cell accelerator voltage for 20*S*-PPD were 461.4 to 425.5, 111 V, 4 eV, and 1 V, respectively. The analytical data were processed using the MassHunter Workstation Software Quantitative Analysis (vB.05.00; Agilent Technologies). The retention time of 20*S*-PPD was 1.09 min. The calibration standard samples were prepared by serial dilution with methanol, thereby yielding a final concentration range of 2.0–1,000 ng/mL. The response of the detector was linear in the concentration range and the mean correlation coefficient ($r^2$) for the calibration curve was more than 0.999. The signal/noise ratio on the lower limit of quantification (LLOQ = 2.0 ng/mL) was higher than 5.0, and there was no interference from any other substance.

Plasma samples containing 20*S*-PPD were allowed to thaw at room temperature for analysis. A 100-μL aliquot of each sample was deproteinized with 1 mL methanol containing 500 ng/mL ketoprofen as an internal standard (IS). After vortexing for 5 min, followed by centrifugation at 16,000*g* for 5 min, a 900-μL aliquot of the supernatant was transferred and evaporated by nitrogen gas at 40°C. Then, the film was reconstituted with 100 μL methanol. After vortexing for 5 min, followed by centrifugation at 16,000*g* for 5 min, the supernatant was injected into an Agilent LC–MS/MS system with the same column and MS/MS conditions. The mobile phase was 88% acetonitrile and 12% water containing 0.2% formic acid (v/v). The flow rate was 0.40 mL/min. The *m/z* value of precursor to product ion, fragment voltage, collision energy, and cell accelerator voltage for 20*S*-PPD were the same as described above. The parameters for IS were 255.1 to 209.1, 110 V, 11 eV, and 1 V, respectively. The retention time of 20*S*-PPD and IS was 1.17 min and 0.51 min, respectively. The calibration standard samples were prepared by spiking the working standard into the blank plasma, thereby yielding a final concentration range of 2.0–1,000 ng/mL. The response of the detector was linear in the concentration range and the mean correlation coefficient ($r^2$) for the calibration curve was over 0.999. The signal/noise ratio at the LLOQ (2.0 ng/mL) was set at 5.0 (Fig. S1).

### 2.9. Statistical analysis

A $p$ value of less than 0.05 was considered statistically significant using the analysis of variance (ANOVA) with Tukey's *post hoc*

test (SAS version 9.4 statistical software; SAS Institute Inc., Cary, NC, United States). All data are expressed as the mean ± standard deviation.

## 3. Results

### 3.1. Preparation of ME formulations

Owing to the poor solubility of 20*S*-PPD in water (36.8 ng/mL), various oils and surfactants were tested to select a more suitable vehicle. The rank of the tested compounds in the order of decreasing solubility of 20*S*-PPD is as follows: Capmul MCM EP > Lauroglycol CC > Labrafac CC as oils and Labrasol > Tween 20 > isopropyl myristate > Limonene > PEG 400 as surfactants (Table 1). The pseudo-ternary phase diagrams consisting of water (DW), oil (Capmul MCM EP), and $S_{mix}$ are shown in Fig. 2. $S_{mix}$ is a mixture of Labrasol and Tween 20 at three different ratios (1:1, 2:1, and 3:1, w/w). As shown in Fig. 2, the formation of clear and transparent ME was confirmed from the pseudo-ternary phase diagrams constructed using all three different $S_{mix}$ ratios. Three different ME formulations were selected from within the clear and transparent area of MEs prepared with the various $S_{mix}$ ratios (F1, F2, and F3).

### 3.2. Physicochemical characterization of 20*S*-PPD-loaded ME and MEH formulations

The compositions of 20*S*-PPD-loaded ME formulations are listed in Table 2. The physicochemical properties, including particle size, polydispersity index, and zeta potential, of 20*S*-PPD-loaded MEs are summarized in Table 3. The mean particle size of the prepared ME formulations ranged from 69.1 nm to 99.6 nm, with F1 having the smallest particle size. When Transcutol HP and soy PC were additionally introduced as cosurfactants, the mean particle size only slightly (not significantly) increased to 106 nm and 110 nm in F4 and F5, respectively. A near-neutral surface charge was observed for all tested 20*S*-PPD-loaded ME formulations. The particle size distribution and TEM images of F1 and F5 showed that spherical and nano-sized particles with a narrow-to-moderate size distribution were observed in 20*S*-PPD-loaded MEs (Fig. 3).

Then, MEH formulations were prepared by the addition of gelling agents, such as xanthan gum, Poloxamer 407, or Carbopol 941, into F5. When adding xanthan gum, a turbid and unclear formulation was observed (Fig. S2A). The rank of the three MEHs in the order of decreasing viscosity was as follows: Carbopol-based MEH (29,400 mPa s) > xanthan gum-based MEH (8,420 mPa s) > Poloxamer-based MEH (657 mPa s). This result was consistent with the fluidity of MEHs observed in a horizontal position (Fig. S2B). As shown in Fig. 3, spherical droplets derived from F5 were located in the Carbopol gel (F5-H), and their droplet sizes seemed to be similar to those of F5. The pH, viscosity, and maximum loading capacity values of the ME and MEH formulations are listed in Table 3. The pH value of F5-H (6.91) was closer to neutral than those of other MEs (5.33 to 5.55). The viscosity was much higher in F5-H (29,400 mPa s) than in other MEs (9.33 mPa s to 11.2 mPa s). There were no significant differences in maximum loading capacity among all the ME and MEH formulations tested, ranging from 3.56 mg/mL to 3.94 mg/mL.

### 3.3. In vitro deposition of 20*S*-PPD in hairless mouse skin and Strat-M membrane

Fig. 4A shows *in vitro* deposition of 20*S*-PPD at 6 h in hairless mouse skin and at 3 h in Strat-M membranes after the topical application of F1, F2, and F3. The deposited amount of 20*S*-PPD at 6 h in the epidermis/dermis of hairless mouse skin was the highest in F1 ($p < 0.01$), whereas there was no significant difference in the SC deposition of 20*S*-PPD among the three ME formulations tested. Moreover, the 20*S*-PPD deposition at 3 h on the Strat-M membrane was higher in F1 than in F3 ($p < 0.05$). Fig. 4B shows the effect of cosurfactants added to the F1. Notably, the deposited amounts of 20*S*-PPD at 6 h in the epidermis/dermis of hairless mouse skin were significantly higher in F4 and F5 than in F1 ($p < 0.05$), whereas there was no significant difference in the SC deposition of 20*S*-PPD among the three ME formulations tested. Moreover, the 20*S*-PPD deposition at 3 h in the Strat-M membrane was the highest in F5 ($p < 0.01$). The *in vitro* deposition of 20*S*-PPD at 3 h in Strat-M membrane after the topical application of the suspension, oil solution, and F5-H formulations is shown in Fig. 5. The deposited amounts of 20*S*-PPD were F5H > oil solution > suspension ($p < 0.001$).

### 3.4. In vivo skin deposition and plasma levels of 20*S*-PPD after the topical administration of the MEH formulation

Figs. 6 and 7 show *in vivo* skin deposition profiles and plasma levels, respectively, of 20*S*-PPD at 3 h, 6 h, 12 h, 18 h, and 24 h after the topical administration of the suspension, oil solution, and F5-H formulations in hairless mice. The *in vivo* skin deposition and plasma levels of 20*S*-PPD tended to increase over time in all of the formulations. The deposited amounts of 20*S*-PPD at 3 h and 6 h in the SC and at 3 h, 6 h, 12 h, 18 h, 24 h in the epidermis/dermis were significantly higher in F5-H than in the two control formulations ($p < 0.01$; Fig. 6). In contrast, there were no significant differences in the plasma concentrations of 20*S*-PPD at 6 h, 12 h, 18 h, and 24 h among all the formulations tested.

### 3.5. Stability of 20*S*-PPD-loaded ME and MEH formulations

The stability of 20*S*-PPD in the oil solution, F1, F5, and F5-H at room temperature and 40°C for 56 d was evaluated in terms of particle size distribution, phase separation/aggregation, and drug content (Table 4 and Fig. S3). As a result, in the oil solution, F5, and F5-H formulations, no aggregates were observed and their transparency was maintained for 56 d. However, the formation of aggregates together with a wide and discrete particle-size

**Table 3**
Physicochemical properties of 20*S*-PPD-loaded ME and MEH formulations

| | Droplet size (nm) | PDI | Zeta potential (mV) | pH | Viscosity (mPa s) | MLC (mg/mL) |
|---|---|---|---|---|---|---|
| F1 | 69.1 ± 2.56 | 0.331 ± 0.006 | −0.353 ± 0.769 | 5.33 ± 0.257 | 10.3 ± 0.211 | 3.28 ± 0.243 |
| F2 | 79.7 ± 1.80 | 0.254 ± 0.030 | −0.590 ± 1.13 | 5.41 ± 0.181 | 9.87 ± 0.493 | 3.79 ± 0.334 |
| F3 | 99.6 ± 2.18 | 0.306 ± 0.028 | −0.740 ± 1.05 | 5.38 ± 0.149 | 9.33 ± 0.785 | 3.94 ± 0.159 |
| F4 | 106 ± 1.10 | 0.347 ± 0.053 | −0.170 ± 0.452 | 5.45 ± 0.248 | 10.4 ± 0.191 | 3.63 ± 0.478 |
| F5 | 110 ± 7.47 | 0.436 ± 0.019 | −1.08 ± 0.217 | 5.55 ± 0.314 | 11.2 ± 0.339 | 3.72 ± 0.562 |
| F5-H | ND | ND | ND | 6.91 ± 0.249 | 29,400 ± 882 | 3.56 ± 0.529 |

ME, microemulsion; MEH, ME-based hydrogel; MLC, maximum loading capacity; ND, no data; PDI, polydispersity index; 20*S*-PPD, 20(*S*)-protopanaxadiol.

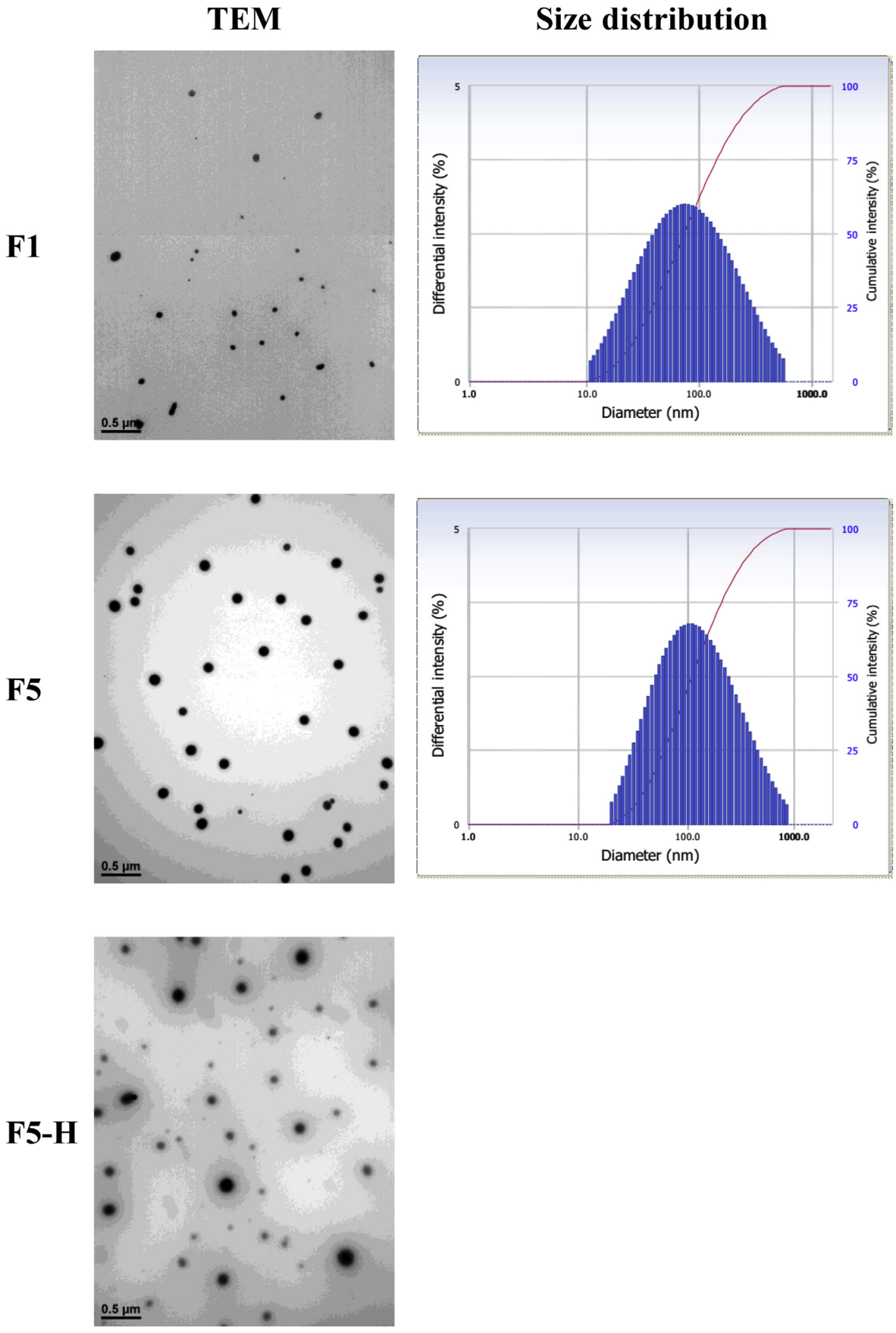


**Fig. 3.** Transmission electron microscopy (TEM) images and particle size distribution of 20S-PPD-loaded ME and MEH formulations. The TEM images were obtained using a LIBRA 120 (Carl Zeiss, Jena, Germany) at 80 kV after staining with 2% phosphotungstic acid. The scale bars represent 0.5 μm. Particle size distributions were obtained using an ELS 8000 (Otsuka Electronics Co. Ltd., Tokyo, Japan) at 25°C. 20S-PPD, 20(*S*)-protopanaxadiol; ME, microemulsion; MEH, ME-based hydrogel.

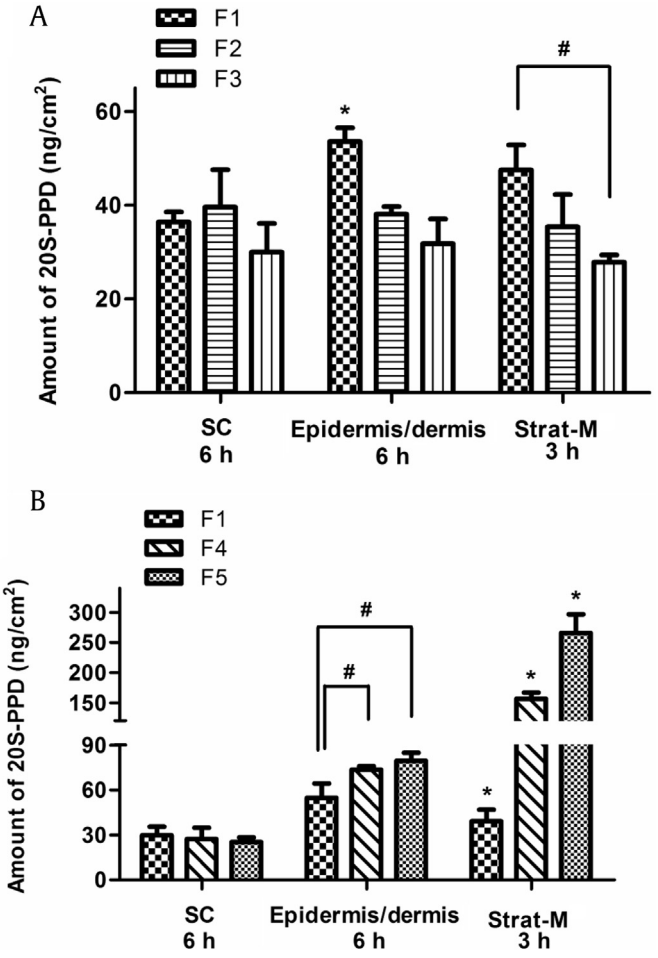


**Fig. 4.** *In vitro* deposition of 20(*S*)-protopanaxadiol (20*S*-PPD) in the stratum corneum (SC) and epidermis/dermis of hairless mouse skin at 6 h and in Strat-M membranes at 3 h after the topical administration of F1–F5 [(A): F1, F2, F3; (B): F4, F5] at a concentration of 0.1% (w/w). The rectangular bars and their error bars represent the means and standard deviations, respectively ($n = 3$). *Significantly different from that of the other groups ($p < 0.05$). #Significant difference between the two groups indicated ($p < 0.05$).

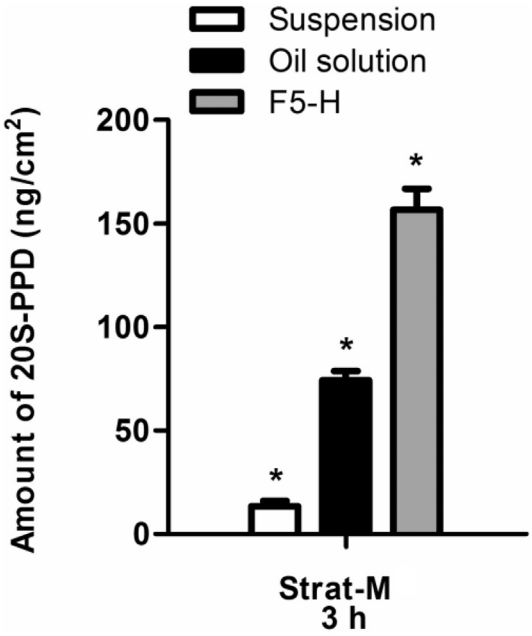


**Fig. 5.** *In vitro* deposition of 20(*S*)-protopanaxadiol (20*S*-PPD) in Strat-M membranes at 3 h after the topical administration of the suspension, oil solution, and F5-H at the 20*S*-PPD concentration of 0.1% (w/w). The rectangular bars and their error bars represent the means and standard deviations, respectively ($n = 3$). *Significantly different from that of the other groups ($p < 0.05$).

distribution was observed in F1 at both temperatures on Day 14, Day 28, and Day 56 after preparation (Fig. S3). Moreover, the 20*S*-PPD content of the oil solution, F5, and F5-H remained nearly constant at both temperatures for 56 d, whereas those of F1 significantly decreased to 67.1% and 68.5% at room temperature and 40°C, respectively (Table 4).

## 4. Discussion

The present study provides novel data on the development of ME and MEH formulations for the topical delivery of a ginsenoside metabolite, 20*S*-PPD. To prepare ME systems in this study, Capmul MCM EP was selected as an oil phase whereas Labrasol and Tween 20 were selected as constituents of the $S_{mix}$ phase, because of their ability to solubilize 20*S*-PPD when compared to the other oils and surfactants tested (Table 1). The selected surfactants have high hydrophilic–lipophilic balance (HLB) values, 14.0 for Labrasol and 16.7 for Tween 20, and are considered as emulsifiers suitable for the formation of oil-in-water MEs [26]. In the pseudo-ternary phase diagram shown in Fig. 2, the three ME formulations (F1–F3) with different Labrasol/Tween 20 ratios were selected based on the principle of high water portion and low $S_{mix}$ portion within the transparent ME region [27,28]. Additionally, Transcutol HP (HLB = 4.2) and soy PC (HLB = 4.5) were used as cosurfactants in the F4 and F5 ME formulations (Table 2) [29]. The combinations of high-HLB surfactants and these low- to medium-HLB cosurfactants are known to render ME systems more stable [26,30]. Moreover, soy PC can increase the flexibility of the oil–water interface, thereby enhancing the physical stability of ME system [31,32]. The maximum loading contents of 20*S*-PPD in all the ME formulations tested were above 3 mg/mL, which was markedly higher in comparison with the aqueous solubility of 20*S*-PPD (36.8 ng/mL). Based on this maximum loading capacity, the loading content of 20*S*-PPD in the ME formulations was set to 0.1% (w/w) for further studies to prevent aggregation and precipitation in the ME system.

To prepare the MEH system, hydrophilic polymers such as xanthan gum, Poloxamer 407, and Carbopol 941 were used as gelling agents. However, the addition of xanthan gum to the ME formulations resulted in an instantaneous aggregate formation and considerably increased turbidity (Fig. S2). This may have been because of an increase in oil–water interfacial tension caused by xanthan gum [12]. Moreover, the viscosities of Poloxamer 407-based MEH formulations (657 mPa s at room temperature and 2,840 mPa s at 32°C) were much lower than 20,000 mPa s, which is generally considered suitable for topical dermal applications [15,33]. Carbopol is a polymer of acrylic acid cross-linked with polyalcohol allyl ethers. As it contains a high proportion of carboxyl groups, its aqueous solution is acidic with a pH of about 3.0 [34]. When the Carbopol solution is neutralized with a basic compound (e.g., triethanolamine used in this study), additional hydrogen ions ($H^+$) are dissociated from the carboxyl groups of Carbopol, and consequently the charge of the polymer chains is changed to be negative. Then, an electrostatic repulsion between the anionic polymer chains can make them maximally uncoiled, resulting in an increased viscosity and swelling, which is called a gelation process [35]. Carbopol has been widely regarded as a useful component of drug delivery gel systems for dermal, ocular, buccal, nasal, and rectal applications [36]. The rheological properties of Carbopol gels,

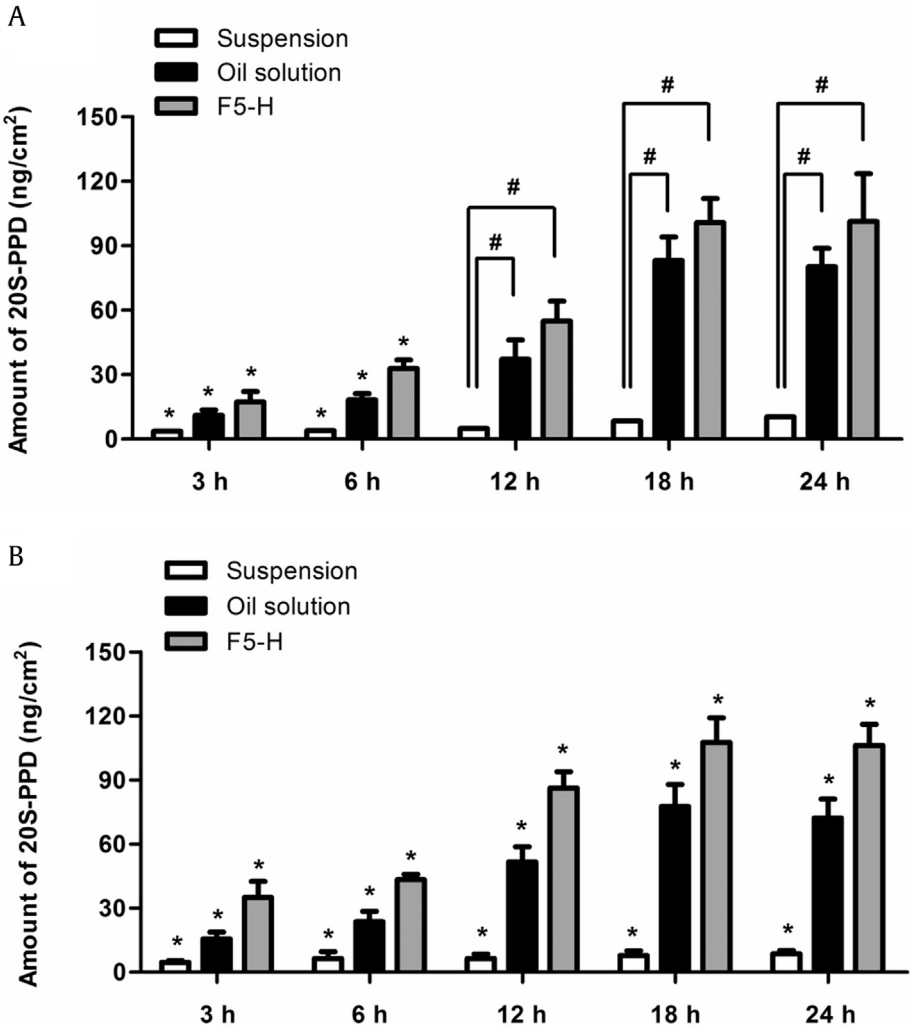


**Fig. 6.** *In vivo* skin deposition of 20(*S*)-protopanaxadiol (20*S*-PPD) at 3 h, 6 h, 12 h, 18 h, and 24 h. (A) In the stratum corneum (SC) of hairless mouse skin after the topical administration of the suspension, oil solution, and F5-H containing 0.1% (w/w) 20*S*-PPD at a dose of 25 mg/kg. (B) In the epidermis/dermis of hairless mouse skin after the topical administration of the suspension, oil solution, and F5-H containing 0.1% (w/w) 20*S*-PPD at a dose of 25 mg/kg. The rectangular bars and their error bars represent the means and standard deviations, respectively ($n = 3$). *Significantly different from that of the other groups ($p < 0.05$). #Significant difference between the two groups indicated ($p < 0.05$).

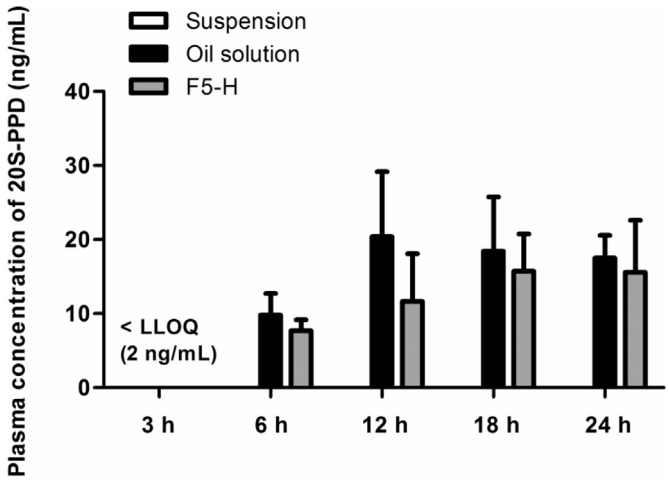


**Fig. 7.** *In vivo* plasma concentration levels of 20(*S*)-protopanaxadiol (20*S*-PPD) 3 h, 6 h, 12 h, 18 h, and 24 h after the topical administration of the suspension, oil solution, and F5-H containing 0.1% (w/w) 20*S*-PPD at a dose of 25 mg/kg in hairless mice. The rectangular bars and their error bars represent the means and standard deviations, respectively ($n = 3$). LLOQ, lower limit of quantification.

including remarkable temperature stability, long relaxation time, and low thixotropy, make them amenable in topical delivery systems requiring prolonged and enhanced skin deposition of a drug [37]. In our study, the prepared MEH formulation containing 1.0% (w/w) Carbopol 941 and 2.0% (w/w) triethanolamine (F5-H) was transparent in appearance and exhibited an appropriate viscosity (29,400 mPa s) for topical dermal applications.

The physicochemical properties of the ME and MEH formulations were characterized as shown in Table 3. The mean droplet sizes of the ME formulations significantly increased as the Labrasol/Tween 20 ratios increased (F1: 69.1 nm → F2: 79.1 nm → F3: 99.6 nm). The mean droplet sizes were further increased by the addition of cosurfactants into the water phase of F1 and resultant increases in oil/water ratios (F4, 106 nm; F5, 110 nm). Notably, TEM images showed that the droplet sizes of F5 seemed to be comparable to those of F5-H (Fig. 3). This result is consistent with a previous study that reported no significant influence of Carbopol on the size and morphology of ME droplets [15,17]. The surface charges of droplets in all formulations prepared were near neutral (Table 3), probably because they consisted of nonionic surfactants and oil. This may reduce the risk of skin irritations that can occur more often in the topical use of charged formulations containing ionic

**Table 4**
Contents (% of initial loading dose) of 20(*S*)-protopanaxadiol (20*S*-PPD) in the oil solution, F1, F5, and F5-H formulations stored at room temperature (RT) or 40°C on 0 d (immediately after preparation), 7 d, 14 d, 28 d, and 56 d

| Time (d) | Oil solution | | F1 | | F5 | | F5-H | |
|---|---|---|---|---|---|---|---|---|
| | RT | 40°C | RT | 40°C | RT | 40°C | RT | 40°C |
| 0 | 98.4 ± 3.54 | 99.1 ± 3.26 | 98.4 ± 1.69 | 100 ± 4.12 | 102 ± 1.28 | 101 ± 0.699 | 98.1 ± 4.58 | 99.3 ± 2.39 |
| 7 | 96.4 ± 4.28 | 104 ± 2.52 | 97.6 ± 3.45 | 98.2 ± 0.842 | 100 ± 6.59 | 101 ± 0.287 | 105 ± 1.12 | 104 ± 1.24 |
| 14 | 90.1 ± 1.78 | 92.8 ± 2.19 | 79.1 ± 1.50 | 81.0 ± 2.99 | 92.0 ± 2.10 | 91.8 ± 3.92 | 96.3 ± 4.20 | 94.9 ± 2.26 |
| 28 | 94.8 ± 2.09 | 92.1 ± 1.99 | 74.0 ± 0.764 | 76.4 ± 2.76 | 94.8 ± 3.14 | 95.6 ± 2.18 | 98.4 ± 1.59 | 101 ± 3.45 |
| 56 | 95.6 ± 3.10 | 94.1 ± 4.18 | 67.1 ± 2.84 | 68.5 ± 3.89 | 95.1 ± 4.15 | 94.8 ± 3.39 | 97.6 ± 3.48 | 97.7 ± 2.49 |

surfactants [38]. The mean pH values of all the ME and MEH formulations ranged from 5.33 to 6.91, which are comparable to a pH value of normal human skin (5.5–6.5) [39]. The viscosities of ME formulations were markedly enhanced by the addition of Carbopol 941, which would be more appropriate for topical administration [17]. In the long-term stability test, F1 was observed to be stable for 7 d but unstable on Day 14 and after that, while F5 was stable through Day 56 (Table 4). This may be attributable to the higher surfactant contents in F5 than in F1, thereby preventing the aggregation or precipitation of poorly soluble ingredients such as 20*S*-PPD.

Owing to a limited availability of human skin and its high variability in lipid and protein compositions depending on body weight, sex, age, and diet, hairless mouse skin has been widely regarded as a useful alternative to human skin [25]. Previous studies have demonstrated a good correlation of skin permeation profiles between human and hairless mouse skin [40]. Among F1, F2, and F3, the deposited amounts of 20*S*-PPD in both the epidermis/dermis of hairless mouse skin and Strat-M membranes were the highest in F1.

Previous studies have reported that the skin permeation and deposition of ME or MEH systems were enhanced as their droplet size decreased [41,42]. Thus, it appears that the smaller droplet size of F1 than F2 and F3 (Table 3) may be responsible for the observations depicted in Fig. 4A, but further investigation is required to understand the exact mechanism(s). Notably, the incorporation of Transcutol as a cosurfactant into F1 significantly enhanced the deposited amounts of 20*S*-PPD in both the epidermis/dermis of hairless mouse skin and the Strat-M membrane (F4 in Fig. 4B). Moreover, the incorporation of soy PC as an additional cosurfactant into F4 further enhanced the deposition of 20*S*-PPD in the Strat-M membrane (F5 in Fig. 4B). Transcutol can act as a skin permeation enhancer by interacting with hydrophilic moieties of skin lipids and proteins [43]. Soy-PC, the main component of cell membranes, can readily fuse with the SC and increase its fluidity, thereby exerting a skin permeation-enhancing effect [32,44]. Thus, it is plausible that the enhancement of skin deposition of 20*S*-PPD observed in F4 and F5 may be attributable to the permeation-enhancing activity of the cosurfactant added. Based on the results shown in Fig. 4, F5 was selected for further studies on the development of MEH formulation.

The *in vitro* deposition of 20*S*-PPD after applying F5-based hydrogels (F5-H) together with the suspension and oil solution formulations (serving as control groups) containing 20*S*-PPD was evaluated using Strat-M membranes. The deposited amount of 20*S*-PPD was significantly higher in F5-H than in the two control groups (Fig. 5). Notably, as shown in Figs. 4B and 5, the Strat-M membrane deposition of 20*S*-PPD in F5-H (157 ± 10 ng/cm$^2$) was significantly lower than that in F5 (266 ± 31 ng/cm$^2$). Although the exact mechanism is unclear, a viscous gel network could have retarded the release of 20*S*-PPD from F5-H, resulting in the reduced deposition. The *in vivo* skin deposition of 20*S*-PPD was evaluated after the topical administration of the suspension, oil solution, and F5-H containing 20*S*-PPD to hairless mice (Fig. 6). At all time points, the extent of *in vivo* epidermal/dermal 20*S*-PPD deposition was suspension < oil solution < F5-H, which showed a similar tendency to the *in vitro* 20*S*-PPD deposition in the Strat-M membranes (Fig. 5). Based on previously proposed mechanisms that explain the enhancing effect of MEs on topical and transdermal drug delivery, it is suggested that the present MEH system may enhance the skin deposition of 20*S*-PPD through the following mechanisms: (1) As only dissolved drug molecule can permeate through the skin, the solubilizing effect of MEH can provide a higher drug loading capacity and larger concentration gradient of the drug toward the skin [45]. (2) The oil and surfactants used in the MEH can diffuse into the skin and act as permeation enhancers by disrupting the lipid structure of the SC and/or increasing the solubility of the drug in the skin, leading to an increase in the partition coefficient of the drug between the formulation and skin [46]. (3) The hydration of the SC by the MEH can reduce the barrier function of the SC and enhance drug transport through the skin [47]. (4) The nano-sized ME droplets can provide a larger surface area available for drug release and diffusion [48].

Recently, it was demonstrated that 20*S*-PPD showed an anti-wrinkle and skin-whitening effect at a concentration range of 250–1,000nM [10]. Assuming that the thickness of the epidermis/dermis layer of male hairless mouse skin is 510 μm [49], the epidermal/dermal concentrations of 20*S*-PPD can be calculated from its deposited amounts. As a result, the calculated epidermal/dermal concentration values at all time points were as follows: 200–274nM in the suspension group, 663–2,180nM in the oil solution group, and 1,490–3,670nM in the F5-H group. In general, drug permeability in human skin tends to be lower by several folds than that in mouse skin [25]. Thus, it can be speculated that the suspension and oil solution formulations cannot provide sufficient epidermal/dermal 20*S*-PPD concentration levels, which implies a potential merit to the MEH formulation developed in this study.

In our preliminary *in vitro* skin permeation study (Fig. S4 and Table S1), the flux and $Q_{24\ h}$ (cumulative amount penetrated over 24 h) of 20*S*-PPD were comparable between the oil solution and F5-H groups (the permeated amount in the suspension group was below the detection limit), whereas the $D_{24\ h}$ (deposited amount at 24 h) of 20*S*-PPD was F5-H > oil solution > suspension both in the SC and epidermis/dermis ($p < 0.05$). In the *in vivo* deposition study, after the topical application of oil solution and F5-H, the plasma concentrations of 20*S*-PPD gradually increased and reached a steady-state level of about 20 ng/mL at 12 h or 18 h (Fig. 7). The time profiles of the deposited 20*S*-PPD amount also exhibited similar tendency to those of the plasma 20*S*-PPD concentrations (Fig. 6). These results can be attributable to a driving force for the permeation of 20*S*-PPD through the skin maintaining over 24 h both in the oil solution and F5-H groups (Fig. S4).

Notably, the results shown in Fig. S4, Figs. 6 and 7, and Table S1 suggest that the F5-H can enhance the *in vitro*/*in vivo* skin deposition of 20*S*-PPD but does not change its *in vitro* skin permeation (flux and $Q_{24\ h}$) and *in vivo* systemic absorption (steady-state

plasma level), when compared with the oil solution. A possible mechanism for this result is a shift of rate-limiting barrier to skin permeation. In a normal condition, the SC, the outermost layer of the skin, provides the main barrier to the skin permeation of compounds with poor solubility and/or permeability like 20*S*-PPD. However, when 20*S*-PPD-loaded oil solution and F5H formulations were applied on the skin, the oil and MEH can reduce the barrier function of the SC and consequently enhance the skin deposition of 20*S*-PPD to different degrees (F5-H > oil solution) depending on their permeation-enhancing mechanisms. Meanwhile, for a topically administered compound to be absorbed into the systemic circulation, the compound should diffuse deeper into more hydrophilic lower parts of the skin and subsequently permeate through the capillary endothelium, even after it has passed the highly lipophilic SC barrier. These conditions can provide an additional rate-limiting barrier against the *in vitro* permeation (from the donor cells into the receptor cells) and *in vivo* systemic absorption (from the skin into the blood) of topically applied 20*S*-PPD that has a high lipophilicity (log $p > 5$) and large molecular size unfavorable for transdermal delivery (460.1 Da). Thus, it is speculated that the shift of rate-limiting barrier from the SC (normal condition) to the lower parts and capillary endothelium of the skin tissue (formulation application) may be responsible for the enhanced deposition and unaltered permeation/systemic absorption of 20*S*-PPD observed in this study. Similarly, several previous studies also reported the discrepancy between skin deposition versus permeation (or systemic absorption) of highly lipophilic and/or relatively large molecular-sized drugs loaded in topical ME, MEH, nanostructured lipid carrier, or nanoemulsion formulations [50–54].

The Strat-M membrane comprises three different polymeric layers with different compositions and structures. The density and rigidness of each layer gradually decrease from the top to the bottom of the membrane to mimic native full-thickness skin [55]. It is well known that Strat-M membrane can be used as a good alternative to animal and human skin in screening tests to estimate the permeability of drugs for transdermal delivery [55]. However, little information is available regarding the relationship between drug deposition profiles in Strat-M membrane and native skin. As shown in Fig. 8B–D, good linear correlations between *in vitro* 20*S*-PPD deposition in the Strat-M membrane and *in vivo* 20*S*-PPD deposition in hairless mice were found by a linear regression analysis of skin deposition data for all formulations studied. Meanwhile, as shown in Figs. 4 and 8A, *in vitro* 20*S*-PPD deposition at 3 h in Strat-M membrane correlated well to that at 6 h in the epidermis/dermis of hairless mouse skin, but not in the SC. However, the exact mechanisms responsible for this result remain unknown because the deposition experiments could not be conducted with each separated layer of Strat-M membrane. Thus, further investigation on the relationship between drug deposition profiles

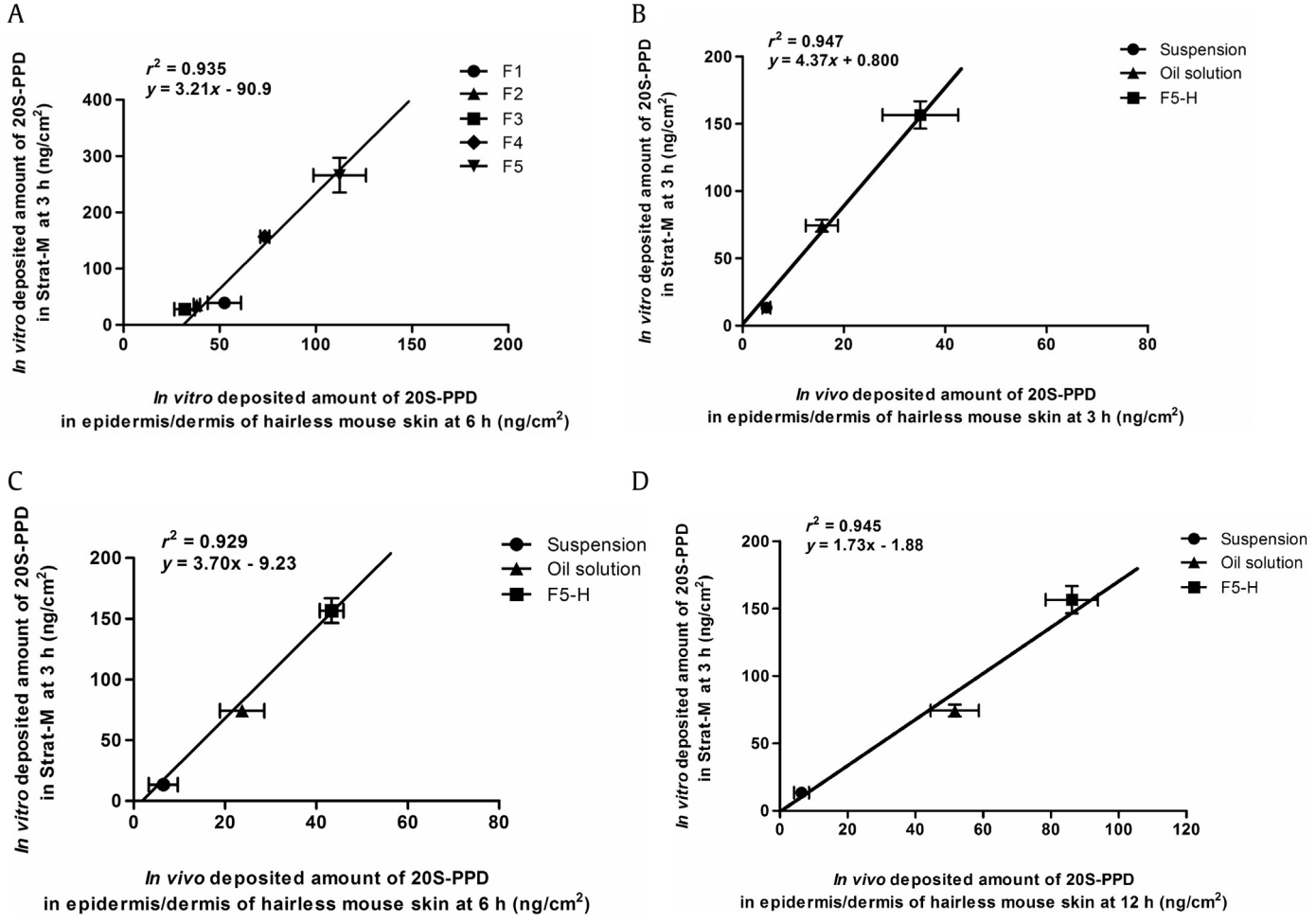


**Fig. 8.** Correlation of the *in vitro* deposited 20(*S*)-protopanaxadiol (20*S*-PPD) amounts at 3 h in Strat-M membranes with the *in vitro* deposited 20*S*-PPD amounts at (A) 6 h and *in vivo* deposited 20*S*-PPD amounts at (B) 3 h, (C) 6 h, and (D) 12 h in the epidermis/dermis of hairless mouse skin. The bullet symbols and their error bars represent the means and standard deviations, respectively ($n = 3$). The solid lines represent the fitted linear regression curves.

in Strat-M membrane and each part (i.e., SC, epidermis, and dermis) of native skin needs to be performed with various drugs and sampling time points.

The contents (w/w%) of oil (Capmul MCM EP, 17.5%), co-surfactants (Transcutol, 5%; soy PC, 1%), and gelling agent (Carbopol, 1%) used in the MEH formulation (F5-H) do not exceed the maximum allowable usage levels of additives in topical formulations recommended by the US Food and Drug Administration (Capmul MCM EP, 20%; Transcutol, 15%; soy PC, 1%; Carbopol, 3.5%). Those of surfactants (Labrasol, 17.5%; Tween 20, 17.5%) were also below the levels used in previously developed topical ME and MEH formulations (Labrasol, 24%; Tween 20, 30.6%) [50,56]. In our present study, following the topical application of the MEH formulation, the epidermal/dermal concentration level of the active ingredient, 20*S*-PPD, was estimated to be 1,490–3,670nM, which is below its no observed adverse effect level (4,000nM) for cytotoxicity in human keratinocytes [10]. Thus, it is plausible that the MEH formulation and its ingredients may exhibit little or no dermal toxicity, but a more systematic evaluation of their dermal toxicity will be required for further clinical development of the MEH formulation.

In conclusion, the Carbopol-based MEH formulations were prepared and evaluated for the topical delivery of a potential skin antiaging agent, 20*S*-PPD. The formulations successfully enhanced the solubility, long-term stability, and *in vitro*/*in vivo* skin deposition of 20*S*-PPD with no influence on its systemic absorption in mice. Notably, it was found that the Strat-M membrane provided skin deposition data well correlated to those obtained from the present *in vitro*/*in vivo* mouse skin studies on 20*S*-PPD. To the best of our knowledge, these results are the first reported data regarding the development of 20*S*-PPD-loaded ME/MEH formulations and their deposition profiles in hairless mouse skin and Strat-M membranes. Taken together, the MEH formulation developed in this study could serve as a potentially effective topical delivery system for poorly soluble ginsenosides and their deglycosylated metabolites, including 20*S*-PPD.

## Conflicts of interest

The authors declare that they have no conflicts of interests.

## Acknowledgments

This work was supported by Nano-Convergence Foundation (www.nanotech2020.org) funded by the Ministry of Science, ICT and Future Planning (MSIP) & the Ministry of Trade, Industry and Energy (MOTIE), Republic of Korea (Project Number: R201602410) and by National Research Foundation of Korea (NRF) grant funded by the MISP (No. 2009-0083533).

## Appendix A. Supplementary data

Supplementary data related to this article can be found at http://dx.doi.org/10.1016/j.jgr.2017.07.005.

## References

[1] Kim K. Effect of ginseng and ginsenosides on melanogenesis and their mechanism of action. J Ginseng Res 2015;39:1–6.
[2] Han J, Lee E, Kim E, Yeom MH, Kwon O, Yoon TH, Lee TR, Kim K. Role of epidermal gamma delta T-cell-derived interleukin 13 in the skin-whitening effect of ginsenoside F1. Exp Dermatol 2014;23:860–2.
[3] Wang L, Lu AP, Yu ZL, Wong RN, Bian ZX, Kwok HH, Yue PY, Zhou LM, Chen H, Xu M, et al. The melanogenesis-inhibitory effect and the percutaneous formulation of ginsenoside Rb1. AAPS PharmSciTech 2014;15:1252–62.
[4] Hong YH, Kim D, Hwang K, Yoo S, Han SY, Jeong S, Kim E, Jeong D, Yoon K, Kim S. Photoaging protective effects of BIOGF1K, a compound K-rich fraction prepared from *Panax ginseng*. J Ginseng Res 2017;41:43–51.
[5] Lin Y, Li Y, Song Z-G, Zhu H, Jin Y-H. The interaction of serum albumin with ginsenoside Rh2 resulted in the downregulation of ginsenoside Rh2 cytotoxicity. J Ginseng Res 2017;41:330–8.
[6] Igami K, Ozawa M, Inoue S, Iohara D, Miyazaki T, Shinoda M, Anraku M, Hirayama F, Uekama K. The formation of an inclusion complex between a metabolite of ginsenoside, compound K and gamma-cyclodextrin and its dissolution characteristics. J Pharm Pharmacol 2016;68:646–54.
[7] Kim EO, Cha KH, Lee EH, Kim SM, Choi SW, Pan CH, Um BH. Bioavailability of ginsenosides from white and red ginsengs in the simulated digestion model. J Agric Food Chem 2014;62:10055–63.
[8] Chen C, Wang L, Cao F, Miao X, Chen T, Chang Q, Zheng Y. Formulation of 20(*S*)-protopanaxadiol nanocrystals to improve oral bioavailability and brain delivery. Int J Pharm 2016;497:239–47.
[9] Ling J, Yu Y, Zhu J, Li Y, Ling L, Wang L, Xu C, Duan G. A highly sensitive HPLC-MS/MS method for quantification of 20(*S*)-protopanaxadiol in human plasma and its application in phase IIa clinical trial of a novel antidepressant agent. J Chromatogr B 2016;1031:214–20.
[10] Han S, Lim TG, Kim JE, Yang H, Oh DK, Yoon Park JH, Yoon Park D, Kim HJ, Rhee YK, Lee KW. The ginsenoside derivative 20(*S*)-protopanaxadiol inhibits solar ultraviolet light-induced matrix metalloproteinase-1 expression. J Cell Biochem 2017. http://dx.doi.org/10.1002/jcb.26023. in press.
[11] Marwah H, Garg T, Goyal AK, Rath G. Permeation enhancer strategies in transdermal drug delivery. Drug Deliv 2016;23:564–78.
[12] Wan T, Xu T, Pan J, Qin M, Pan W, Zhang G, Wu Z, Wu C, Xu Y. Microemulsion based gel for topical dermal delivery of pseudolaric acid B: *in vitro* and *in vivo* evaluation. Int J Pharm 2015;493:111–20.
[13] Cavalcanti AL, Reis MY, Silva GC, Ramalho IM, Guimaraes GP, Silva JA, Saraiva KL, Damasceno BP. Microemulsion for topical application of pentoxifylline: *in vitro* release and *in vivo* evaluation. Int J Pharm 2016;506:351–60.
[14] Carvalho AL, Silva JA, Lira AA, Conceicao TM, Nunes Rde S, de Albuquerque Junior RL, Sarmento VH, Leal LB, de Santana DP. Evaluation of microemulsion and lamellar liquid crystalline systems for transdermal zidovudine delivery. J Pharm Sci 2016;105:2188–93.
[15] Zhu W, Guo C, Yu A, Gao Y, Cao F, Zhai G. Microemulsion-based hydrogel formulation of penciclovir for topical delivery. Int J Pharm 2009;378:152–8.
[16] Kansagra H, Mallick S. Microemulsion-based antifungal gel of luliconazole for dermatophyte infections: formulation, characterization and efficacy studies. J Pharm Invest 2016;46:21–8.
[17] Chen H, Chang X, Du D, Li J, Xu H, Yang X. Microemulsion-based hydrogel formulation of ibuprofen for topical delivery. Int J Pharm 2006;315:52–8.
[18] Patel MR, Patel RB, Parikh JR, Patel BG. Formulation consideration and skin retention study of microemulsion containing tazarotene for targeted therapy of acne. J Pharm Invest 2016;46:55–66.
[19] Hathout RM, Mansour S, Geneidi AS, Mortada ND. Visualization, dermatopharmacokinetic analysis and monitoring the conformational effects of a microemulsion formulation in the skin stratum corneum. J Colloid Interface Sci 2011;354:124–30.
[20] Rao S, Barot T, Rajesh K, Jha LL. Formulation, optimization and evaluation of microemulsion based gel of butenafine hydrochloride for topical delivery by using simplex lattice mixture design. J Pharm Invest 2016;46:1–12.
[21] Jaiswal M, Kumar A, Sharma S. Nanoemulsions loaded Carbopol® 934 based gel for intranasal delivery of neuroprotective *Centella asiatica* extract: *in-vitro* and *ex-vivo* permeation study. J Pharm Invest 2016;46:79–89.
[22] El-Sherbiny IM, Yacoub MH. Hydrogel scaffolds for tissue engineering: progress and challenges. Glob Cardiol Sci Pract 2013;2013:316–42.
[23] Lee SG, Kang JB, Kim SR, Kim CJ, Yeom DW, Yoon HY, Kwak SS, Choi YW. Enhanced topical delivery of tacrolimus by a carbomer hydrogel formulation with transcutol P. Drug Dev Ind Pharm 2016;42:1636–42.
[24] Pham CV, Cho C-W. Application of d-α-tocopheryl polyethylene glycol 1000 succinate (TPGS) in transdermal and topical drug delivery systems (TDDS). J Pharm Invest 2017;47:111–21.
[25] Jung E, Kang YP, Yoon IS, Kim JS, Kwon SW, Chung SJ, Shim CK, Kim DD. Effect of permeation enhancers on transdermal delivery of fluoxetine: *in vitro* and *in vivo* evaluation. Int J Pharm 2013;456:362–9.
[26] Lawrence MJ, Rees GD. Microemulsion-based media as novel drug delivery systems. Adv Drug Deliv Rev 2000;45:89–121.
[27] Kim JE, Yoon IS, Cho HJ, Kim DH, Choi YH, Kim DD. Emulsion-based colloidal nanosystems for oral delivery of doxorubicin: improved intestinal paracellular absorption and alleviated cardiotoxicity. Int J Pharm 2014;464:117–26.
[28] Kim KT, Lee J-Y, Park J-H, Cho H-J, Yoon I-S, Kim D-D. Capmul MCM/Solutol HS15-based microemulsion for enhanced oral bioavailability of rebamipide. J Nanosci Nanotechnol 2017;17:2340–4.
[29] da Silva GB, Scarpa MV, Carlos IZ, Quilles MB, Lia RC, do Egito ES, de Oliveira AG. Oil-in-water biocompatible microemulsion as a carrier for the antitumor drug compound methyl dihydrojasmonate. Int J Nanomed 2015;10:585–94.
[30] Silva AE, Barratt G, Cheron M, Egito ES. Development of oil-in-water microemulsions for the oral delivery of amphotericin B. Int J Pharm 2013;454:641–8.
[31] Aloisio C, Longhi MR, De Oliveira AG. Development and characterization of a biocompatible soybean oil-based microemulsion for the delivery of poorly water-soluble drugs. J Pharm Sci 2015;104:3535–43.

[32] Fricker G, Kromp T, Wendel A, Blume A, Zirkel J, Rebmann H, Setzer C, Quinkert RO, Martin F, Muller-Goymann C. Phospholipids and lipid-based formulations in oral drug delivery. Pharm Res 2010;27:1469–86.
[33] Chen H, Mou D, Du D, Chang X, Zhu D, Liu J, Xu H, Yang X. Hydrogel-thickened microemulsion for topical administration of drug molecule at an extremely low concentration. Int J Pharm 2007;341:78–84.
[34] Karthikeyan K, Durgadevi R, Saravanan K, Shivsankar K, Usha S, Saravanan M. Formulation of bioadhesive carbomer gel incorporating drug-loaded gelatin microspheres for periodontal therapy. Trop J Pharm Res 2012;11:335–43.
[35] Suhaime IHB, Tripathy M, Mohamed MS, Majeed ABA. The pharmaceutical applications of carbomer. Asian J Pharm Sci Res 2012;2:1–12.
[36] Tamburic S, Craig DQ. The effects of ageing on the rheological, dielectric and mucoadhesive properties of poly(acrylic acid) gel systems. Pharm Res 1996;13:279–83.
[37] Islam MT, Rodriguez-Hornedo N, Ciotti S, Ackermann C. Rheological characterization of topical carbomer gels neutralized to different pH. Pharm Res 2004;21:1192–9.
[38] Yuan C, Xu Z, Fan M, Liu H, Xie Y, Zhu T. Study on characteristics and harm of surfactants. J Chem Pharm Res 2014;6:2233–7.
[39] Ohman H, Vahlquist A. *In vivo* studies concerning a pH gradient in human stratum corneum and upper epidermis. Acta Derm Venereol 1994;74:375–9.
[40] Jung EC, Maibach HI. Animal models for percutaneous absorption. J Appl Toxicol 2015;35:1–10.
[41] Mou D, Chen H, Du D, Mao C, Wan J, Xu H, Yang X. Hydrogel-thickened nanoemulsion system for topical delivery of lipophilic drugs. Int J Pharm 2008;353:270–6.
[42] Chen L, Tan F, Wang J, Liu F. Microemulsion: a novel transdermal delivery system to facilitate skin penetration of indomethacin. Pharmazie 2012;67:319–23.
[43] Mura P, Faucci MT, Bramanti G, Corti P. Evaluation of transcutol as a clonazepam transdermal permeation enhancer from hydrophilic gel formulations. Eur J Pharm Sci 2000;9:365–72.
[44] Valenta C, Wanka M, Heidlas J. Evaluation of novel soya–lecithin formulations for dermal use containing ketoprofen as a model drug. J Control Rel 2000;63:165–73.
[45] Heuschkel S, Goebel A, Neubert RH. Microemulsions–modern colloidal carrier for dermal and transdermal drug delivery. J Pharm Sci 2008;97:603–31.
[46] Kreilgaard M. Influence of microemulsions on cutaneous drug delivery. Adv Drug Deliv Rev 2002;54:S77–98.
[47] Talegaonkar S, Azeem A, Ahmad FJ, Khar RK, Pathan SA, Khan ZI. Microemulsions: a novel approach to enhanced drug delivery. Recent Pat Drug Deliv Formul 2008;2:238–57.
[48] Ita K. Progress in the use of microemulsions for transdermal and dermal drug delivery. Pharm Dev Technol 2017;22:467–75.
[49] Azzi L, El-Alfy M, Martel C, Labrie F. Gender differences in mouse skin morphology and specific effects of sex steroids and dehydroepiandrosterone. J Invest Dermatol 2005;124:22–7.
[50] Patel MR, Patel RB, Parikh JR, Patel BG. Novel isotretinoin microemulsion-based gel for targeted topical therapy of acne: formulation consideration, skin retention and skin irritation studies. Appl Nanosci 2016;6:539–53.
[51] Kong X, Zhao Y, Quan P, Fang L. Development of a topical ointment of betamethasone dipropionate loaded nanostructured lipid carrier. Asian J Pharm Sci 2016;11:248–54.
[52] Naz Z, Ahmad FJ. Curcumin-loaded colloidal carrier system: formulation optimization, mechanistic insight, *ex vivo* and *in vivo* evaluation. Int J Nanomedicine 2015;10:4293–307.
[53] Fan X, Chen J, Shen Q. Docetaxel–nicotinamide complex-loaded nanostructured lipid carriers for transdermal delivery. Int J Pharm 2013;458:296–304.
[54] Sah AK, Jain SK, Pandey RS. Microemulsion based hydrogel formulation of methoxsalen for the effective treatment of psoriasis. Asian J Pharm Clin Res 2011;4:140–5.
[55] Uchida T, Kadhum WR, Kanai S, Todo H, Oshizaka T, Sugibayashi K. Prediction of skin permeation by chemical compounds using the artificial membrane, Strat-M. Eur J Pharm Sci 2015;67:113–8.
[56] Idrees M, Rahman N, Ahmad S, Ali M, Ahmad I. Enhance transdermal delivery of flurbiprofen via microemulsions: effects of different types of surfactants and cosurfactants. Daru 2011;19:433–9.